SAND2013-3670C

Optimal Resistive Control Strategy for a Floating OWC Device Considering Both the Oscillating Structure and the Oscillating Water Column

Diana Bull[1], Erick Johnson[2]

[1]*Sandia National Laboratories*
Albuquerque, NM, USA
dlbull@sandia.gov

[2]*Montana State University*
Bozeman, MT, USA
erick.johnson@me.montana.edu

***Abstract*—A linear, frequency-domain, performance model is presented that links an oscillating structure to air-pressure fluctuations with a Wells Turbine in 3-dimensions for a floating OWC device. An array of field points defining the interior free surface allows hydrodynamic parameters relating to the fluctuating air-pressure within the OWC to be calculated using reciprocity relations after analysis with a potential flow solver. Device structural parameters for a non-optimized BBDB are detailed and the performance model is exercised on this device. The hydrodynamically coupled resonance location of the OWC is identified. Power values for two optimization cases are presented. The first optimization case considers only the power absorbed by the fluctuating air-pressure, while the second case considers the power absorbed by both the oscillating structure and the fluctuating air-pressure. In both cases the optimal resistive damping and the resulting performance are presented. Comparison of these two optimizations shows a 30% increase in power conversion in monochromatic waves when both the oscillating structure and the fluctuating air-pressure are considered in the optimization procedure.**

***Keywords*—wave energy, OWC, moonpool, BBDB, 3-dimensional frequency domain performance model, resistive damping control, Wells Turbine**

I. INTRODUCTION

An oscillating water column (OWC) is a class of wave energy converter (WEC). Essentially this WEC contains a moonpool, an opening in a partially submerged structure, with an air chamber covering the free surface. The air chamber is only open to the atmosphere through a turbine. The incident waves result in a fluctuating pressure within the air chamber. Bidirectional air flow, caused by the difference in pressure within the chamber relative to the ambient outside, drives the turbine and produces power. Often a self-rectifying turbine, like the Wells Turbine, is employed so that the turbine rotates only in one direction.

OWCs can be located offshore (OE Buoy [1], blueWAVE [2], Sperboy [3]), nearshore (greenWAVE [2]), or onshore (Pico [4], Limpet [5], Mutriku [6]). The deployment location strongly affects the requirements on the performance model. An offshore OWC will have to float, which uniquely requires that both the wave activated body and the OWC are modeled in a coupled fashion as each absorbs power from the waves. It is the relative motion between the device and the internal free surface that produces air flow in this case. Nearshore and onshore OWCs only require the pressure fluctuation from the internal free surface to be modeled, thus reducing the number of independent variables to be considered.

Additionally the OWC can absorb energy either as a terminator or a point absorber. This directional dependence in energy absorption identifies the theoretical limits of conversion. When evaluating a floating OWC, the directional dependence impacts the wave activated body motions. Hence, quite distinct body oscillations and power absorptions are expected between these two directional dependences.

In this paper an offshore (floating) OWC terminator is studied. The Backward Bent Duct Buoy (BBDB) design was first proposed by Masuda [7] in the 1980's and is one variety of floating OWC devices. This design is an L-shape with the opening to the ocean downstream from the wave propagation direction. The BBDB benefits from the coupled surge, heave, and pitch rigid-body modes and the OWC's resonance to expand the frequency range of efficient conversion. The natural resonance of the OWC is dependent upon both the length and free surface area of the water column [8] [9].

There are two approaches to modeling the free surface: a rigid weightless piston [10] or calculation of the pressure distribution [11] [12]. The first approach is only valid for small internal free surface areas and is akin to a 2-body treatment in which the oscillating structure and the OWC are treated independently. The second approach does not place limitations on the size of the internal free surface area and utilizes a Boundary Element Method (BEM) solver to model the dynamics of the floating body and the fluctuating air-pressure. Calculation of the internal pressure distribution can be obtained in three ways: approximated, solved for explicitly, or solved for implicitly [13] [14]. Approximation utilizes the technique of generalized modes [13] which expands upon the rigid piston approximation to include additional higher order modes. Explicit calculation requires determination of the velocity potential for the free surface. This is currently

possible in WAMIT v7.0 [15], however this capability is new and uncommon in other potential flow solvers. Implicit calculation utilizes reciprocity relations to solve for all of the free surface parameters from the oscillating structure potential using an array of field points on the internal free surface. Implicit calculation, presented in [14] and [16] and applied by [17], is pursued in this paper allowing for the use of standard potential flow solvers, such as WAMIT v6.4 [18].

This paper will present a general BBDB design in Section II in order to discuss the 3-dimensional hydrodynamic model and results presented in Sections III and IV respectively. Section V develops the performance model, linked through a Wells Turbine, as well as two optimization procedures. Section VI presents the effects of optimizing resistive control of the Wells Turbine considering only power absorbed by the fluctuating air-pressure versus considering power absorbed by both the oscillating structure and fluctuating air-pressure. The two methodologies are compared in a monochromatic environment.

II. Floating OWC Geometry

The BBDB is modeled to determine both the structural parameters, using SolidWorks [19], as well as the hydrodynamic parameters, using MultiSurf [20]. Fig. 1 illustrates the structural design, while Fig. 2 shows the hydrodynamic counterpart (note only the wetted surface must be modeled for the potential flow BEM solver). The majority of the device dimensions were selected based upon the conclusions of the following papers [21], [22], and [23]. This design profile is not optimized to reduce viscous losses or encourage weathervaning as is depicted in [1] and [17].

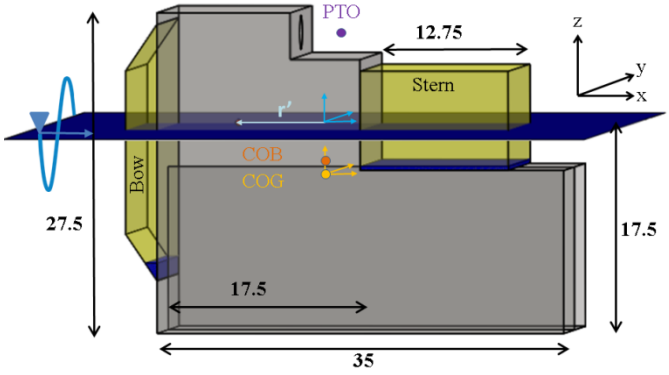

Fig. 1. Model of the OWC describing dimensions, locations of principal components, locations of the COB and COG, and identifying coordinate systems

The structural design assumes a uniform thickness of A36 steel, appropriate ballast mass and placement, and an estimate of the mass and location of the power conversion chain. An average wall thickness of 35.1 mm is applied to the entire device [24]. This average thickness was derived from a structural design engineered to withstand the hydrostatic pressure at a submergence of 25 m [25]. The ballast is distributed to obtain the desired draft and ensure that the center of gravity and the center of buoyancy are aligned vertically. The ballast is assumed to be seawater and is added to the buoyancy chambers as shown in Fig. 1. The mass of the power conversion chain (drivetrain, generator, power conditioning electronics) is approximated [26] and is placed at the expected center of the Wells Turbine location, also shown in Fig. 1. TABLE I summarizes the structural properties of the device that are needed as input into WAMIT [18].

Displaced Mass [kg]		2,024,657		
Structural Mass [kg]		1,808,944		
Bow Ballast Mass [kg]		22,072		
Stern Ballast Mass [kg]		123,641		
Power Conversion Mass [kg]		70,000		
COG (x,y,z) [m]		0.00	0.00	-4.29
COB (x,y,z) [m]		0.00	0.00	-3.31
Free Surface Center (x,y,z) [m]		-5.12	0.00	0.00
Radius of Gyration at COG [m]	x	12.53	0.00	0.00
	y	0.00	14.33	0.00
	z	0.00	0.00	14.54

TABLE I. Structural properties of the device

The global and body coordinate systems adopted for the hydrodynamic model are identified in Fig. 1. The global coordinate system is identified in blue in Fig. 1 and is at the undisturbed water level directly above the body coordinate system. The incident wave velocity potential φ_o, and hence the phases of the exciting forces, are defined relative to the global coordinate system. The body panels shown in Fig. 2 are defined relative to the center of gravity (COG), which defines the location of the body coordinate system identified in gold in Fig. 1. The body forces and motions calculated by WAMIT are calculated relative to this coordinate system.

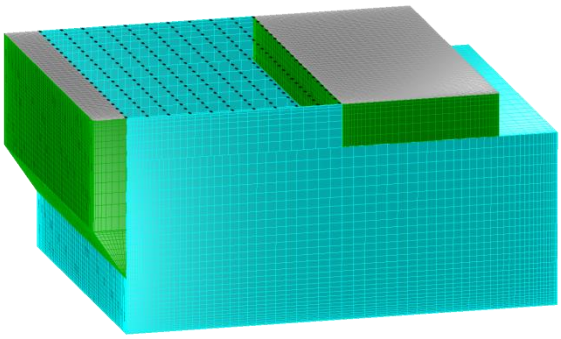

Fig. 2. Wetted surface geometry modeled with cosine spacing in MultiSurf. Dipole panels (cyan), conventional body panels (green), interior surfaces for irregular frequency removal (gray). Black points illustrate the interior field point locations.

Panels representing the 3-dimensional wetted surface of the BBDB are used by the BEM potential flow solver. Fig. 2 illustrates the discretization of panels as well as the types of panels used to solve for the hydrodynamic parameters. The structure panels, green, calculate the wave source potential to obtain the velocity potential. The dipole panels, cyan, obtain the velocity potential without calculation of the source potential. While the grey panels facilitate the removal of irregular frequencies that result from the calculation of the source potential when there is a large waterplane area. Cosine

spacing is applied to the panels to increase the accuracy of the calculations close to the corners. The panels are analyzed using the higher-order method. Only half of the device is modeled due to the device plane of symmetry at $y = 0$.

An array of 231 field points describing the interior free surface of the BBDB is defined with respect to the global coordinate system. This array is illustrated in Fig. 2 with black points. The field points capture the dynamic pressure and velocity distributions of the free surface.

III. Hydrodynamic Formalism: Reciprocity Relations

Using linear potential flow theory to describe wave structure interactions for a floating OWC, the velocity potential of i moving bodies oscillating in all rigid body modes j with k internal free surfaces is given by

$$\hat{\phi} = \hat{\phi}_o + \hat{\phi}_d + \sum_{ij} \varphi_{ij} \hat{u}_{ij} + \sum_{k} \varphi_k \hat{p}_k \qquad 1$$

following the notation of [16]. The hat, $\widehat{\ }$, indicates complex amplitudes. The total velocity potential given in Eq. 1 is composed of the incident $\hat{\phi}_o$ and diffracted $\hat{\phi}_d$ potentials as well as the body $\sum_{ij} \varphi_{ij} \hat{u}_{ij}$ and free surface $\sum_k \varphi_k \hat{p}_k$ radiation potentials. The device treated in this paper contains only one body and one free surface, as shown in Fig. 1, thus $k = i = 1$. From this point forward, the velocity potentials, hydrodynamic terms, incident wave amplitude, body velocity, and pressure above the free surface are treated with frequency dependent complex amplitudes and sinusoidal time-dependence $e^{i\omega t}$. Thus hat's, $\widehat{\ }$, will no longer be employed to indicate complex amplitudes.

Given that the state of the floating oscillating water column shown in Fig. 1 must be specified by two parameters, the velocity of the moving body and the pressure in the air chamber, it is clear that there are two coupled hydrodynamic equations relating the total force acting on the body and the total volume flow resulting from air-pressure fluctuations. Each of these equations will be composed of the superposition of the excitation solution found from the incident and diffracted potentials, the radiation solution found from the radiation potentials, and a coupling term uniting them together.

Hence, the total hydrodynamic force, F_{TH}, acting on the j^{th} mode of the body is given by the combination of the excitation force f_j found by holding the body fixed in that direction ($u_j = 0$), the radiated force $\sum_{j'} Z_{jj'} u_{j'}$ found by unit-oscillation velocity $u_{j'}$ of the body without altering the pressure ($p = 0$), and a coupling force H_j^p that accounts for unit-fluctuation of the air-pressure inducing body oscillations:

$$F_{TH,j} = f_j A - \sum_{j'} Z_{jj'} u_{j'} - H_j^p p \qquad j = 1, \dots, 6. \qquad 2$$

In Eq. 2, A is the incident wave amplitude at the global origin and $Z_{jj'}$ is the radiation impedance of the j^{th} mode due to unit-oscillation in the j' direction.

The total hydrodynamic volume flow, Q_{TH}, resulting from air-pressure fluctuations is given by the excitation volume flow q found by holding the internal free surface fixed ($p = 0$), the radiated volume flow Yp found by unit-fluctuation of the pressure p without allowing the body to oscillate ($u_j = 0$), and a coupling force H_j^u that accounts for unit-oscillation velocities inducing air-pressure fluctuations:

$$Q_{TH} = qA - Yp - \sum_j H_j^u u_j. \qquad 3$$

In Eq. 3 Y is the radiation admittance of the free surface and is analogous to the radiation impedance for the oscillating structure.

As will be shown below, each of the hydrodynamic terms identified above can be obtained from a potential flow code without explicitly solving for the radiation potential of the free surface. In this paper WAMIT v6.4 [18] is used to obtain the frequency and directionally dependent hydrodynamic terms.

A. The Floating Body

The hydrodynamic terms relating to a freely oscillating structure are derived using portions of the velocity potential defined in Eq. 1 and they are all standard output of WAMIT v6.4. The excitation force f_j is obtained by:

$$f_j = -i\omega\rho \frac{1}{A} \iint_{S_b} (\phi_o + \phi_d) n_j dS \qquad 4$$

where ω is the angular frequency, ρ is the density of seawater, S_b is the wetted surface of the body, and n_j is the unit normal vector pointing into the body. The radiation impedance is found through:

$$Z_{jj'} = i\omega\rho \iint_{S_b} \varphi_j \frac{\partial \varphi_{j'}}{\partial n} dS = b_{jj'} + i\omega a_{jj'} \qquad 5$$

where $b_{jj'} = \mathrm{Re}\{Z_{jj'}\}$ is the radiation resistance and $\omega a_{jj'} = \mathrm{Im}\{Z_{jj'}\}$ is the radiation reactance. Although the radiation potential φ_j is solved for explicitly in WAMIT v6.4, it is important to note that the solution can be found without the explicit potential. The radiation resistance can be found indirectly through a reciprocity relation with the excitation force [16, Eq. 5.148]. And the added mass can be found from the radiation resistance through the Kramers-Kronig relationship [14, Eq. 5.105]. The coupling term H_j^p that results from unit-fluctuations of the air-pressure resulting in body movements is found through

$$H_j^p = i\omega\rho \iint_{S_b} \varphi n_j \, dS \qquad 6$$

where φ is understood to be φ_k with $k = 1$.

Note that the signs of Eq.'s 4, 5, and 6 are switched from the formalism developed in [16] since the unit normal vector must point into the body as a result of the formulation within WAMIT v6.4.

B. The Free Surface

The hydrodynamic terms relating to air-pressure fluctuations above the internal free surface can also be found by using portions of the velocity potential defined in Eq. 1. The excitation volume flow is found through

$$q = \frac{1}{A}\iint_S \frac{\partial(\phi_o + \phi_d)}{\partial z} dS \qquad 7$$

where the integral is taken over the internal free surface S. This integration is computed discretely by obtaining the excitation vertical velocities, $\frac{\partial(\phi_o+\phi_d)}{\partial z}$, at each field point shown in Fig. 2 from WAMIT. The radiation admittance is obtained explicitly through

$$Y = -\iint_S \frac{\partial \varphi}{\partial z} dS = G + iB \qquad 8$$

where $G = \mathrm{Re}\{Y\}$ and $B = \mathrm{Im}\{Y\}$ are the radiation conductance and radiation susceptance of the internal free surface respectively. Analogous to Eq. 5 above, solution for the radiation admittance does not require the explicit radiation potential, φ. As presented in [17], the radiation conductance is related to the excitation volume flow through the following reciprocity relationship

$$G = \frac{2k}{8\pi\rho g v_g}\int_0^{\pi} |q(\beta)|^2 \, d\beta \qquad 9$$

where the integration from 0 to π already acknowledges the transverse symmetry of the device, β defines the incident wave-headings, and v_g is the group velocity. The radiation susceptance can then be found from the radiation conductance through the Kramers-Kronig relationship

$$B(\omega) = -\frac{2\omega}{\pi}\int_0^{\infty} \frac{G(y)}{\omega^2 - y^2} dy \qquad 10$$

where the integral is to be understood in the principal value sense and is most readily evaluated with a Hilbert Transformation. The coupling term H_j^u that results from unit-oscillation velocities resulting in air-pressure fluctuations is found through

$$H_j^u = -\iint_S \frac{\partial \varphi_j}{\partial z} dS = C_j + iJ_j \qquad 11$$

where the integral is taken over the internal free surface S. This integration is computed discretely by obtaining the radiation vertical velocities $\frac{\partial \varphi_j}{\partial z}$ at each field point shown in Fig. 2 from WAMIT. WAMIT User Manual v6.4 in Section 4.7 does not state the correct dimensionalization of the radiation velocities; however this has been corrected in User Manual v7.0. The correct non-dimensionalization for the radiation velocity due to the j^{th} mode is:

$$\overline{\nabla\varphi}_j = \frac{\omega^2 LU}{gL^n u_j} \qquad 12$$

where L is a scaling factor representative of the length of the device defined in the input files, n is dictated by the rigid mode j ($n = 0$ for $j = 1,2,3$ and $n = 1$ for $j = 4,5,6$), and U/u_j is the non-dimensional velocity in the j^{th} mode.

Finally it can be shown that $H_j^p = -H_j^u$ and hence solving Eq. 6, the only hydrodynamic parameter that requires an explicit form of the velocity potential of the free surface, is not necessary.

Body motions and forces are defined relative to the body coordinate system (i.e. the COG) and therefore, a transformation vector is required to account for the velocity of the body at the center of the free surface in the global coordinate system due to body motions around the COG. Thus the vertical velocity of the body at the center of the internal free surface is calculated through multiplication of the body velocity with the transformation vector

$$\boldsymbol{T} = [0 \quad 0 \quad 1 \quad 0 \quad -r' \quad 0]^{\mathrm{T}} \qquad 13$$

where r' is identified in Fig. 1 and TABLE I.

IV. Hydrodynamic Results

The hydrodynamic parameters are found for wave frequencies spanning 0 to 2.5 rad/s in 0.01 rad/s intervals assuming infinite depth. The integral in Eq. 9 requires a sum over incident wave propagations. Therefore hydrodynamic parameters are found for 17 distinct wave-headings starting with incidence in the positive x-direction ($\beta = 0$) and increasing in intervals of $\pi/16$. However, the only wave-heading analyzed to estimate performance is $\beta = 0$.

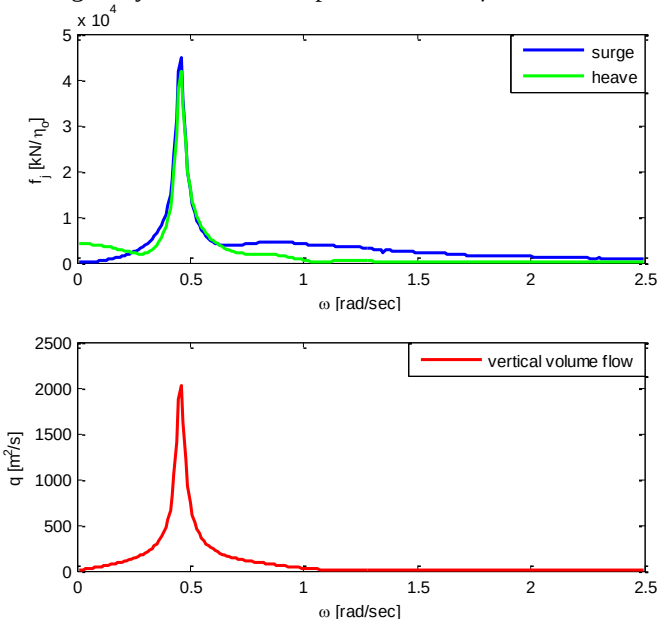

Fig. 3: Excitation forces on the structure in heave and surge as well as the excitation volume flow of the free surface.

Fig. 3 shows the initial excitations from the incident and diffracted velocity potentials for both the oscillating structure f_j in heave and surge as well as the fluctuating volume flow q. Fig. 4 and Fig. 5 show the non-dimensionalized heave and pitch damping terms and added mass/inertia respectively. Unlike axisymmetric devices, non-axisymmetric devices exhibit a cross-coupling between the heave-pitch and the heave-surge rigid body modes, hence the radiation impedance cross-coupling terms are non-zero and appreciable for this device. These cross-couplings influence the locations of the natural resonances of the freely floating structure [27]. Furthermore, the hydrodynamic coupling between the structure and air column is derived from the radiation potential, φ_j, thus we expect from Eq.'s 3 and 11 that both

surge and pitch will contribute to the air-pressure fluctuation through the coupling term H_j^u.

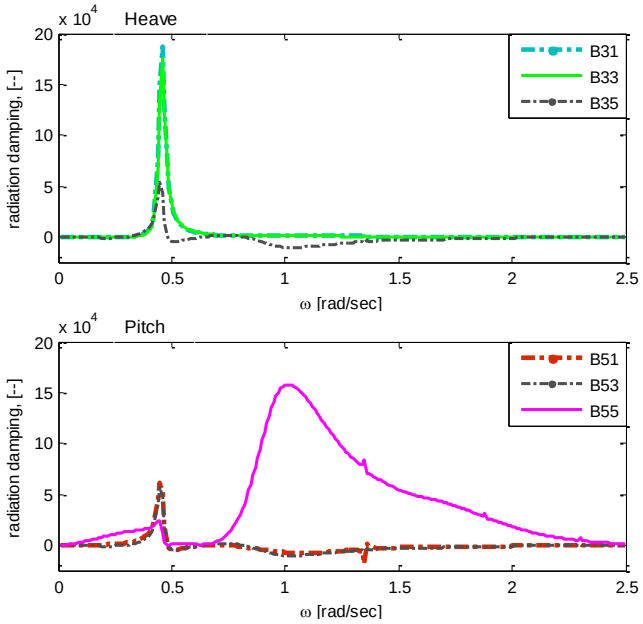

Fig. 4: Non-dimensional radiation damping as a function of frequency for heave and pitch.

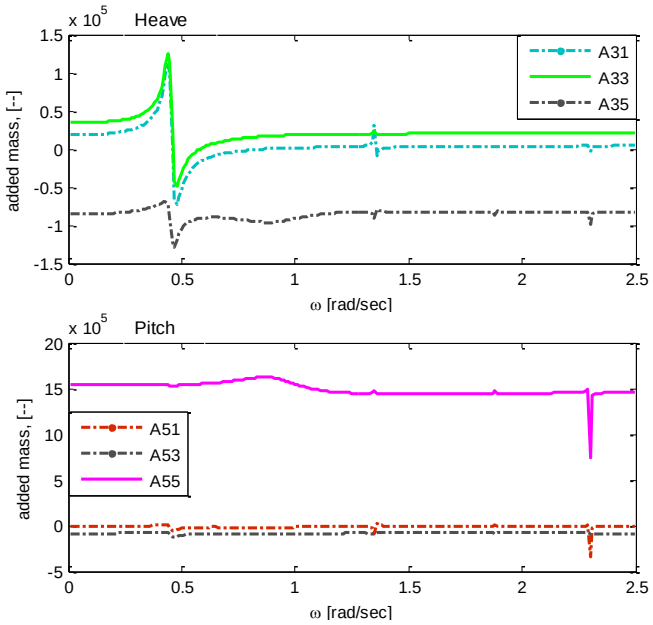

Fig. 5: Non-dimensional added mass/inertia as a function of frequency for heave and pitch.

Fig. 6 shows the real and imaginary components of the heave and pitch coupling terms H_j^u. As expected the magnitude of coupling is quite large in each mode indicating that an oscillating structure will induce a measurable air-pressure fluctuation, or equivalently an air-pressure fluctuation will induce structure motions.

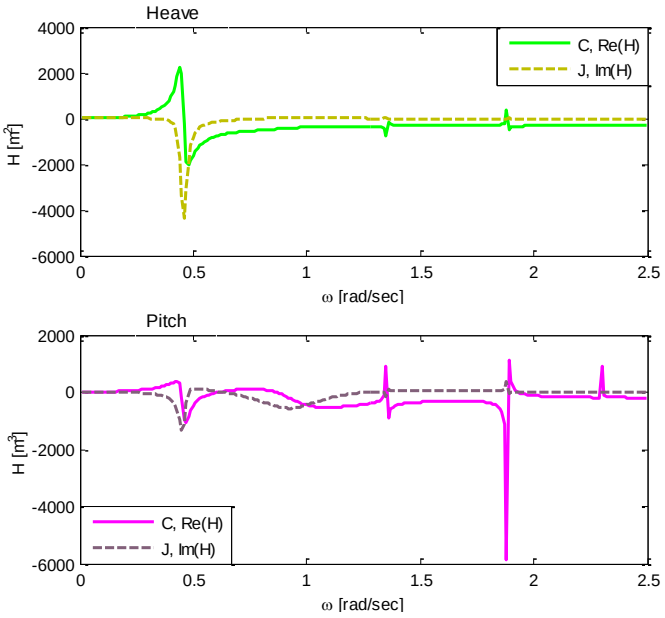

Fig. 6: Coupling terms for heave and pitch motions of the body showing strongly coupling to the fluctuating air-pressure.

The radiation conductance and susceptance are shown in Fig. 7. The large peaks occurring in Fig. 3-Fig. 7 are localized in frequency with the first zero crossing of the radiation susceptance. Since the radiation susceptance includes the effect of the hydrostatic stiffness [16], the first zero crossing is identified as the piston resonance location of the hydrodynamically uncoupled system. However, the resonances of the OWC contained in a floating body are not solely defined by the excitation q and radiation admittance Y. They are additionally influenced by the coupling term $H_j^u u_j$ (see Eq. 3). The non-zero contribution of H_3^u and H_5^u seen in Fig. 6 signify that the natural resonances of the OWC will be influenced by these coupling terms in addition to H_1^u.

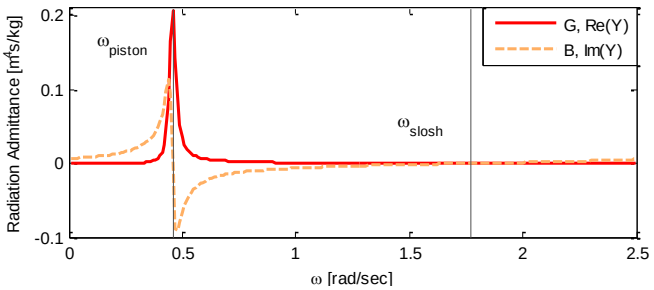

Fig. 7: Radiation conductance and susceptance of the fluctuating air-pressure. The hydrodynamically uncoupled piston and slosh resonances are identified

V. Linked Governing Equations for Floating OWC

A linear frequency-domain model is used to produce estimates of the power conversion capabilities of the device presented in Fig. 1. There are two governing equations: one for the oscillating structure and one for the fluctuating air-pressure. The power conversion chain (Wells Turbine) links

the oscillating structure to the OWC through the resistive damping term R_{load}. The governing equation for each mode of the oscillating structure is given by

$$\begin{aligned} &i\omega m_{jj'}u_j \\ &= \left(f_j A - \left(b_{jj'} + i\omega a_{jj'}\right)u_j - \left(-H_j^u + T_j S\right)p\right) \\ &- \left(\frac{1}{i\omega}C_{jj'}u_j\right) - \left(\frac{1}{i\omega}K_j u_j\right) - \left(b_{vis,j}u_j\right) \end{aligned} \quad (14)$$

where the left-hand side of the equation is the total force acting on the body. The first term on the right-hand side is the hydrodynamic contribution discussed in previous sections with one modification: the coupling term H_j^u is modified by the transformation vector $\boldsymbol{TS}$ to account for the pressure-volume flow that occurs due to the velocity of the body at the center of the free surface. The second term, technically part of the full hydrodynamic contribution, is the hydrostatic restoring force. The third and fourth terms are added to account for additional forces affecting the device: the mooring restoring force and the linearized viscous damping both represented here as diagonal matrices.

A Wells Turbine, which possesses a linear relationship between pressure and flow, is assumed in this performance model. Since air is highly compressible, accurate predictions of the air flow through the Wells Turbine require a linear representation of this compressibility. The governing equation for the relative air flow through the Wells Turbine is given by

$$\begin{aligned} &\left(\frac{1}{R_{load}} + i\frac{\omega\forall_o}{\gamma p_{atm}}\right)p \\ &= \left(qA - (G + iB)p - \sum_j \left(H_j^u + T_j S\right)u_j\right) \\ &- \frac{1}{R_{vis}}p \end{aligned} \quad (15)$$

where the left-hand side of the equation is the total compressible relative air flow through the Wells Turbine (consistent with [28]) with no limitation on the pressure allowed within the air chamber. The linearized air compressibility is defined through the following terms: the initial volume is $\forall_o$, $\gamma = 1.4$ and is the ratio between the constant-pressure and constant-volume specific heats for air, and p_{atm} is the atmospheric pressure. The first term on the right-hand side is the hydrodynamic contribution, discussed in previous sections, modified to include the coupling term, as was similarly done in Eq. 14. The second term is added to account for the viscous damping in a linearized manner.

These coupled governing equations are most readily understood in matrix notation as follows

$$\begin{pmatrix}\boldsymbol{f}\\ q\end{pmatrix}A = \begin{pmatrix}\boldsymbol{Z}_i & \boldsymbol{H}_i \\ \boldsymbol{H}_i^T & Y_i + \frac{1}{R_{load}}\end{pmatrix}\begin{pmatrix}\boldsymbol{u}\\ p\end{pmatrix} \quad (16)$$

where the bolded quantities are matrices or column vectors and

$$\begin{aligned} \boldsymbol{Z}_i &= \boldsymbol{b} + \boldsymbol{b}_{vis} + i\omega\left(\boldsymbol{m} + \boldsymbol{a} - \frac{(\boldsymbol{C} + \boldsymbol{K})}{\omega^2}\right) \\ &= \boldsymbol{\varepsilon} + i\boldsymbol{\theta}, \end{aligned} \quad (17)$$

$$\boldsymbol{H}_i = \boldsymbol{H} + \boldsymbol{T}S = \boldsymbol{\tau} + i\boldsymbol{\psi}, \text{ and} \quad (18)$$

$$Y_i = \left(G + \left(\frac{1}{R_{vis}}\right)\right) + i\left(B + \frac{\omega\forall_o}{\gamma p_{atm}}\right) = \alpha + i\delta. \quad (19)$$

The linked governing equations above can then be solved to obtain the linked body velocity response amplitude operator (RAO) and the linked relative pressure RAO. The relative volume flow through the Wells Turbine may be derived from

$$Q_T = qA - Y_i p - \boldsymbol{H}_i^T\boldsymbol{u} = \frac{1}{R_{load}}p. \quad (20)$$

From the relative volume flow, the relative interior free surface elevation may then be derived from

$$\frac{\xi_{\text{Rel,FSE}}}{A} = -\frac{Q_T/A}{i\omega S}. \quad (21)$$

The negative sign in Eq. 21 reflects the fact that positive volume flow into the chamber occurs for a decreasing free surface elevation.

The instantaneous pneumatic power available to the Wells Turbine will be the product of the relative pressure in the chamber and the relative volume flow. The mean converted power may then be obtained through the following relationship, as presented in [16]

$$\langle P\rangle = \overline{p(t)Q_T(t)} = \frac{1}{2}Re\{pQ_T^*\}. \quad (22)$$

In monochromatic waves and applying the relationship presented in Eq. 22, this relationship simplifies to

$$\langle \mathrm{P}\rangle = \frac{1}{2}\frac{1}{R_{load}}|p|^2. \quad (23)$$

Selection of R_{load} will influence the final delivered power. However, optimization of R_{load} relates to the power absorbed by the WEC. In cases where there is only one radiation potential, the power absorbed by the radiating body/free surface and the mechanical/pneumatic power is equivalent. However, in cases where there are two radiation potentials then the power absorbed by the system is distinct from the mechanical/pneumatic power converted at the drivetrain.

A. Optimal Resistive Damping: Air Chamber Only

If only the power absorbed by the interior free surface is considered, hence ignoring the power absorbed by the oscillating structure, then Eq. 23 represents both the power absorbed by the OWC as well as the pneumatic power at the Wells Turbine. The optimal resistive damping term may then be found from the solution to the following optimization condition

$$\frac{\partial\langle \mathrm{P}\rangle}{\partial\, 1/R_{load}} = 0 \quad (24)$$

where the average absorbed power $\langle P \rangle$ is given by Eq. 23. Solution to this optimization condition results in the frequency dependent optimal resistive damping

$$R_{l_{opt,air}} = \left(\left(G + \frac{1}{R_{vis}} \right)^2 + \left(B + \frac{\omega \forall_o}{\gamma p_{atm}} \right)^2 \right)^{-\frac{1}{2}}. \quad 25$$

Inserting Eq. 25 into Eq. 23 produces the maximum pneumatic power in monochromatic waves. The form of $R_{l_{opt,air}}$ is analogous to that of a single oscillating structure [16, Eq. 3.40]. However, note that inserting Eq. 25 into Eq. 23 is creating a "hybrid" solution. Even though $R_{l_{opt,air}}$ does not recognize the influence of the oscillating structure, the pressure in Eq. 23 is derived from the hydrodynamically coupled system.

B. Optimal Resistive Damping: Body and Air Chamber

If, instead, the power absorbed by the system considers both the oscillating structure as well as the interior free surface, then the absorbed power is distinct from Eq. 23. In this case, the average absorbed power assumes the following relationship, as presented in [16]

$$\langle P_A \rangle = \frac{1}{2} Re\{\boldsymbol{F}_T \boldsymbol{u}^*\} + \frac{1}{2} Re\{p Q_T^*\} \quad 26$$

where the total force acting on the body is defined by the equilibrium condition applied to Eq. 14 and the total volume flow through the turbine is defined by Eq. 20. Following the work of [16], Eq. 26 can be further simplified into the following form

$$\langle P_A \rangle = \frac{1}{4} (\boldsymbol{\kappa}^T \boldsymbol{v}^* + \boldsymbol{\kappa}^\dagger \boldsymbol{v}) - \frac{1}{2} \boldsymbol{v}^\dagger \mathbf{R} \boldsymbol{v} \quad 27$$

where the † represents the complex conjugate and transpose of the matrix, and

$$\boldsymbol{\kappa} = \begin{bmatrix} \boldsymbol{F}_T \\ Q_T \end{bmatrix}, \quad 28$$

$$\boldsymbol{v} = \begin{bmatrix} \boldsymbol{u} \\ -p \end{bmatrix} \quad 29$$

where $\boldsymbol{u}$ and p are found through solution of Eq. 16, and

$$\mathbf{R} = \begin{bmatrix} \boldsymbol{\varepsilon} & -i\boldsymbol{\psi} \\ \boldsymbol{\psi} & \alpha + \frac{1}{R_{load}} \end{bmatrix} \quad 30$$

where $\boldsymbol{\varepsilon}$, $\boldsymbol{\psi}$, and α are defined in Eq.'s 17-19. The relationship presented in Eq. 27 accounts for the power absorbed by the system as a whole. The same optimization condition presented in Eq. 24 can be applied to Eq. 27 to obtain the optimal resistive damping that takes into account both the power absorbed by the oscillating structure as well as the power absorbed by the air chamber. Although an analytic solution in the form of Eq. 25 is not presented here, numeric solution to this optimization problem is presented in Section VI.

VI. Performance Results: Monochromatic Waves

For the results presented below, neither viscous damping on the structure or the free surface is applied: $\boldsymbol{b}_{vis} = 0$ and $1/R_{vis} = 0$. Additionally, no mooring restoring force is applied, hence $\boldsymbol{K} = 0$.

A. Optimal Resistive Damping: Air Chamber Only

Fig. 8 shows $R_{l_{opt,air}}$ from Eq. 25 as a function of frequency when only the power absorbed by the oscillating water column is considered. As expected, $R_{l_{opt,air}}$ is minimal at the hydrodynamically uncoupled piston resonance location identified as the *B* zero-crossing location in Fig. 7. On either side of the expected resonance location $R_{l_{opt,air}}$ rises resulting in one resistive damping peak.

Fig. 9 compares the linked and unlinked RAO's for heave, pitch, and the absolute free surface elevation when $R_{l_{opt,air}}$ is applied at all frequencies. In the unlinked RAO plots, the structural resonances are identified. It is evident that adding the power conversion chain to link the two systems through the influence of R_{load} has a strong impact on the expected responses. In the linked case, both the heave and pitch resonances disappear while a new peak appears corresponding to increased resistive damping. The relative-linked pressure is shown in Fig. 10. The peaks in pressure correspond to increased resistive damping, while the peaks in relative volume flow (not shown) correspond to resonances.

B. Optimal Resistive Damping: Body and Air Chamber

Fig. 11 shows the optimal R_{load} obtained when absorbed power accounts for both the body oscillations and the free surface fluctuations; this will be referred to as $R_{l_{opt,body+air}}$. Since both the body motions and the free surface resonance are accounted for in this treatment, the profile of $R_{l_{opt,body+air}}$ experiences 2 distinct minima at the structural resonances. The structural resonance locations are again identified in Fig. 11 for clarity. Between these minima, $R_{l_{opt,body+air}}$ increases resulting in three resistive damping peaks.

Fig. 12 compares the linked and unlinked RAO's for heave, pitch, and the absolute free surface elevation when $R_{l_{opt,body+air}}$ is applied at all frequencies. The linked RAO's show both of the unlinked structural resonances as well as two new peaks that correspond to the increased resistive damping seen in $R_{l_{opt,body+air}}$. The relative-linked pressure is shown in Fig. 13. Again, the peaks in pressure occur with the increased resistive damping.

Work by Alves [29] has shown the effect of accounting for both the oscillating structure and the fluctuating air-pressure with a one-dimensional, axisymmetric, floating OWC device modeled using generalized modes. Although the governing equations are simplified in this one-dimensional model, Alves also numerically optimizes Eq. 27. His results are similar showing a new peak between the structural heave resonance and the OWC piston resonance. This third peak is the combined heave-piston peak that is the result of both the body and the fluctuating air-pressure oscillating in phase but with distinct amplitudes.

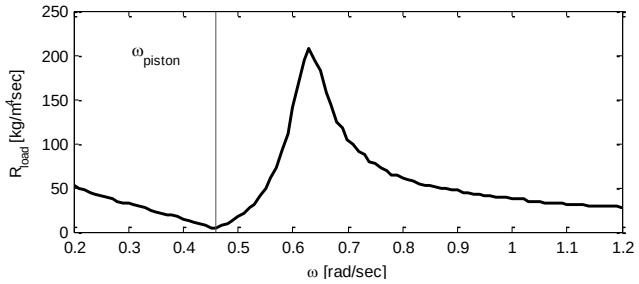

Fig. 8: Optimal resistive damping when considering only the OWC, $\boldsymbol{R}_{l_{opt,air}}$.

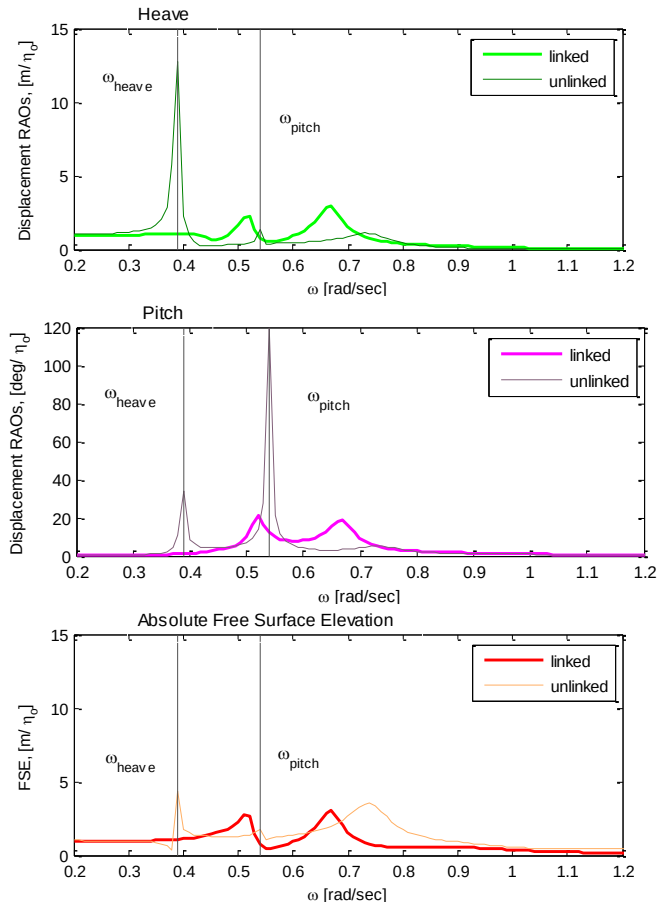

Fig. 9: RAO's for heave, pitch, and the absolute free surface elevation when a Wells Turbine with $\boldsymbol{R}_{l_{opt,air}}$ is applied in the linked case and when there is no Wells Turbine in the unlinked case.

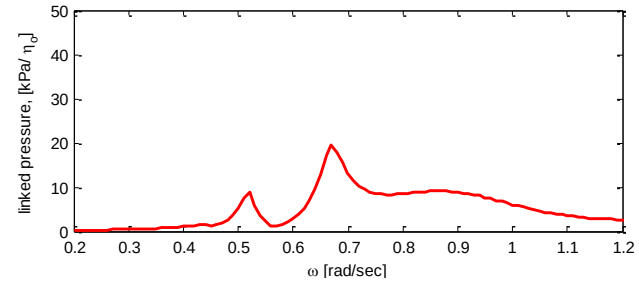

Fig. 10: RAO of relative linked pressure with $\boldsymbol{R}_{l_{opt,air}}$ applied.

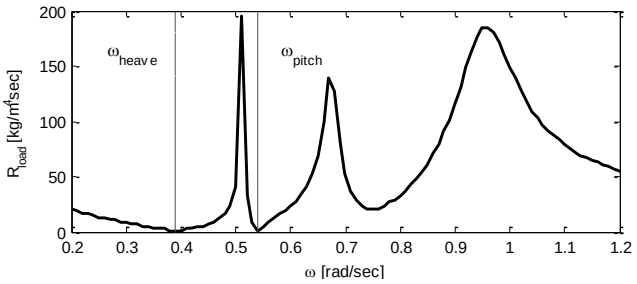

Fig. 11: Optimal resistive damping when considering only the oscillating structure and the OWC, $\boldsymbol{R}_{l_{opt,body+air}}$.

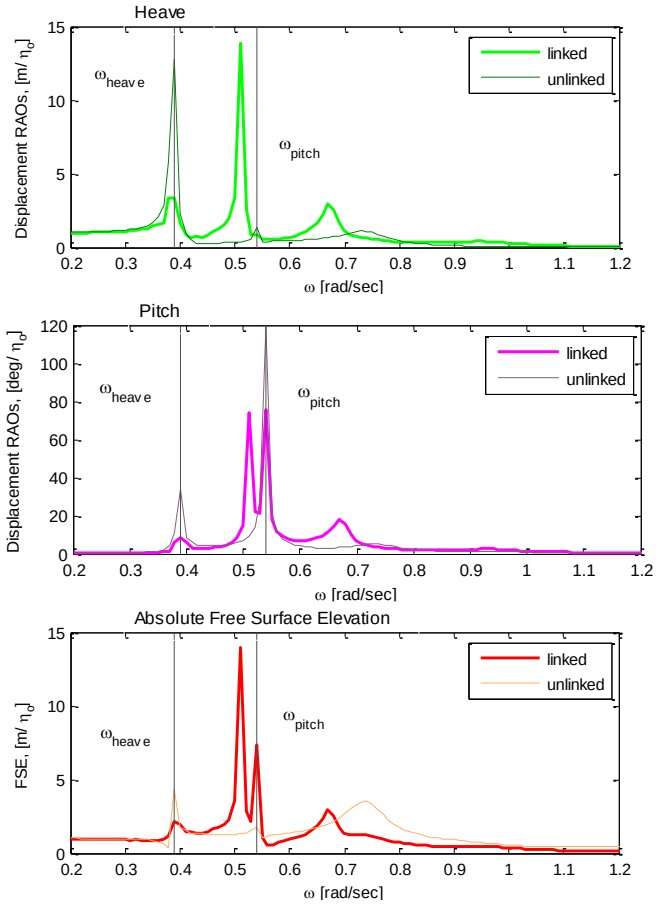

Fig. 12: RAO's for heave, pitch, and the absolute free surface elevation when a Wells Turbine with $\boldsymbol{R}_{l_{opt,body+air}}$ is applied in the linked case and when there is no Wells Turbine in the unlinked case.

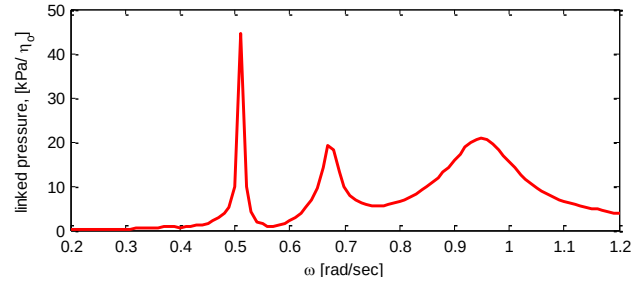

Fig. 13: RAO of relative linked pressure $\boldsymbol{R}_{l_{opt,body+air}}$ applied.

When considering the results from Alves in combination with Fig. 11-Fig. 13, it appears that the OWC resonance of the fluctuating air-pressure in this hydrodynamically coupled system is located at $\omega = 0.73$ and not at the B zero-crossing. Inspection of Fig. 11 shows minimal damping at $\omega = 0.73$ due to the large unlinked RAO responses seen in Fig. 12. Further, since the response of the fluctuating air-pressure is now dependent upon the coupling terms, as discussed in Section IV, the resulting fluctuating air-pressure resonance could migrate due to the coupling with surge, heave, and pitch structural modes in much the same way that the heave structural resonance migrates due to the influence of the rigid-body cross-coupling terms. Additionally, the phase shift introduced through r' in Fig. 1 changes the incorporation of the hydrodynamically coupled air column resonance. Fig. 14 shows the magnitude and phase of the hydrodynamically coupled, but unlinked, pressure RAO numerator, $q - \boldsymbol{u}\boldsymbol{H}_i^T$.

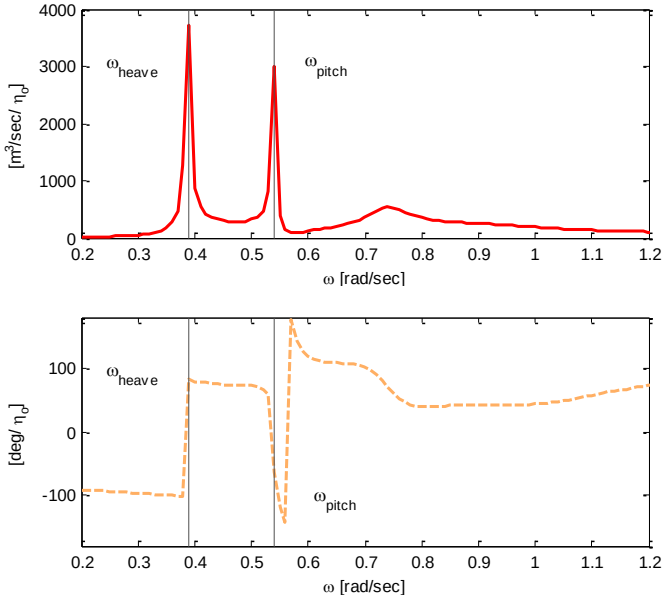

Fig. 14: Numerator of hydrodynamically coupled, but unlinked, pressure RAO. Magnitude of peak and phase change at $\omega = 0.73$ indicate's the OWC resonance location for the hydrodynamically coupled system.

The soft OWC resonance at $\omega = 0.73$ corresponds to a steady change in phase; this type of resonance is often associated with damped systems. In this case, the non-zero B would offer this damping.

C. Comparison

Fig. 15 compares the pneumatic power available for each of these optimization strategies, and demonstrates the importance of accounting for the power absorbed by the oscillating structure in combination with the OWC. The total absorbed power (i.e. the area under each of the curves in Fig. 15**)** with $R_{l_{opt,air}}$ applied at each frequency is 41 MW. Whereas the similar measure for $R_{l_{opt,body+air}}$ is 59 MW. Although these power values could not be realistically achieved, they are a useful metric for comparison. Thus, by accounting for the power absorbed by the oscillating structure, there is a 30% increase in predicted power available to the Wells Turbine.

The structures of the linked RAOs and the optimal R_{load}'s display the underlying cause in this difference in power. By ignoring power absorbed by the oscillating structure the optimal $R_{l_{opt,air}}$ has only one minima at the location of the hydrodynamically uncoupled piston resonance shown in Fig. 7. Thus, the heave and pitch resonances clearly seen in the unlinked RAOs are unable to manifest themselves because an appreciable $R_{l_{opt,air}}$ damps out the natural structural resonances. This optimization strategy results in a narrower frequency range of conversion and hence less overall power.

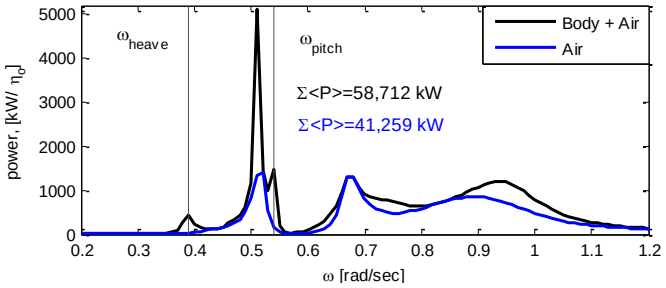

Fig. 15: RAO of power through the Wells Turbine for both optimization cases: $\boldsymbol{R}_{\boldsymbol{l}_{\boldsymbol{opt,body+air}}}$ (black) and $\boldsymbol{R}_{\boldsymbol{l}_{\boldsymbol{opt,air}}}$ (blue).

Conversely $R_{l_{opt,body+air}}$ has minima corresponding to the structural resonances. Thus, the resonances seen in the unlinked RAOs are maintained in the linked RAO structures. Additionally, between these natural structural resonances two additional responses, driven by $R_{l_{opt,body+air}}$, are found. Therefore, linking the structure to the OWC through the Wells Turbine has allowed for additional power to be converted through these combined heave-OWC and pitch-OWC peaks. Hence, only by accounting for the oscillating structure and air-pressure fluctuations within the OWC will the full advantages of the BBDB design be capitalized upon.

Although coupling between the structure and the OWC is often mentioned as a benefit of the BBDB design, this is the first presentation, to the authors' knowledge, demonstrating the combined heave-OWC and pitch-OWC modes. These combined modes expand the area of power conversion.

VII. Conclusions

A linear, frequency-domain, performance model is presented that links the oscillating structure to air-pressure fluctuations with a Wells Turbine in 3-dimensions for a floating OWC device. The hydrodynamic parameters related to the fluctuating air-pressure within the OWC are calculated using reciprocity relations on an array of field points defining the interior free surface.

Device structural parameters for a non-optimized BBDB are detailed to aid in comparative studies. Dimensions of the device were informed from literature while the structural properties were obtained from an idealized solid model. The performance model is exercised on this device using the

calculated hydrodynamic parameters. The air is modeled as a compressible system.

Power curves are presented for two optimization cases when the structure is linked to the fluctuating air-pressure through a Wells Turbine. The first optimization case considers the power absorbed by the fluctuating air-pressure only. The second optimization case considers the power absorbed by both the fluctuating air-pressure and the oscillating structure. In both cases the optimal resistive damping as a function of frequency is presented as well as the performance model results. Results include RAO's of the device motion and internal free surface height as well as the pressure in the chamber and the pneumatic power available to the turbine. Comparison of these two optimizations show a 30% increased power conversion in monochromatic waves when both the oscillating structure and the fluctuating air-pressure are considered in the optimization procedure.

Results presented here indicate that cross-coupling between the oscillating structure and the fluctuating air-pressure combine to move the OWC resonance from the first *B* zero-crossing in a similar manner as rigid-body cross-coupling moves the primary structural resonances.

These results are conclusive in showing the need to optimize the resistive damping of a floating OWC considering the power absorbed by both the oscillating structure and the fluctuating air-pressure. However, no device operates linearly, without viscous losses, nor in monochromatic waves. Further work expanding the analysis to spectral treatments of the climate and incorporating viscous losses is currently being pursued to ensure the consistency of the conclusion.

ACKNOWLEDGMENT

The author would like to acknowledge helpful conversations with Adi Kurniawan, Paul Palo, Marco Alves, and staff at HMRC. The author would like to acknowledge clarifications from WAMIT's Nick Newman and Chang-Ho Lee. Additionally the author would like to acknowledge the help of Guild Copeland in the creation of solid models.

This work was funded by the Department of Energies' Wind and Water Power Technologies Office. Sandia National Laboratories is a multi-program laboratory managed and operated by Sandia Corporation, a wholly owned subsidiary of Lockheed Martin Corporation, for the U.S. Department of Energy's National Nuclear Security Administration under contract DE-AC04-94AL85000.

REFERENCES

[1] Ocean Energy Ltd., "Ocean Energy OEBuoy: A Backward Bent Duct Design." [Online]. Available: http://www.oceanenergy.ie/. [Accessed: 04-Apr-2013].

[2] Oceanlinx Ltd., "Oceanlins'x blueWAVE (offshore) and greenWAVE (nearshore)." [Online]. Available: http://www.oceanlinx.com/. [Accessed: 19-Apr-2013].

[3] Embley Energy Ltd., "Embley Energy's Sperboy." [Online]. Available: http://www.sperboy.com. [Accessed: 19-Apr-2013].

[4] A. F. de O. Falcao, "The shoreline OWC wave power plant at the Azores," presented at the 4th European Wave Energy Conference, Aalborg, Denmark, 2000.

[5] Heath, T, Whittaker, TJT, and Boake, CB, "The design, construction and operation of the LIMPET wave energy converter (Islay, Scotland)," presented at the 4th European Wave Energy Conference, Aalborg, Denmark, 2000.

[6] Y. Torre-Enciso, I. Ortubia, L. I. López de Aguileta, and J. Marqués, "Mutriku wave power plant: from the thinking out to the reality," in *Proceedings 8th European Wave Tidal Energy Conference*, 2009, pp. 319–29.

[7] Y. Masuda, T. Yamazaki, Y. Outa, and M. McCormick, "Study of backward bent duct buoy," in *OCEANS'87*, 1987, pp. 384–389.

[8] Fukuda, K., "Behaviour of water in vertical well with bottom opening of ship, and its effect on ship motions," *Journal of Naval Architects of Japan*, vol. 141, pp. 107–122, 1977.

[9] Y. Wei, J. Yang, G. Chen, and Z. Hu, "The Research of Moonpool Size Effect on the Hydrodynamic Performance of FDPSO," in *Proceedings of the ASME 2011 30th International Conference on Ocean, Offshore and Arctic Engineering*, Rotterdam, The Netherlands, 2011, pp. 459–467.

[10] D. V. Evans, "The Oscillating Water Column Wave-energy Device," *IMA J Appl Math*, vol. 22, no. 4, pp. 423–433, Dec. 1978.

[11] D. V. Evans, "Wave-Power Absorption by Systems of Oscillating Surface Pressure Distributions," *Journal of Fluid Mechanics*, vol. 114, pp. 481–499, 1982.

[12] A. J. N. A. Sarmento and A. F. de O. Falcão, "Wave generation by an oscillating surface-pressure and its application in wave-energy extraction," *Journal of Fluid Mechanics*, vol. 150, pp. 467–485, 1985.

[13] Lee, C.-H., Newman J.N., and Nielsen F.G., "Wave interactions with an oscillating water column," in *Proceedings International Offshores and Polar Engineering Conference*, Los Angeles, 1996.

[14] C. H. Lee and F. G. Nielson, "Analysis of oscillating-water column device using a panel method.pdf," presented at the 11th International Workshop on Water Waves and Floating Bodies, Hamburg Germany, 1996.

[15] *WAMIT v7.0*. Chestnut Hill, Massachusetts: WAMIT, Inc.

[16] Johannes Falnes, *Ocean Waves and Oscillating Systems*. New York: Cambridge University Press, 2002.

[17] Kurniawan, A, Hals, J, and Moan, Torgeir, "Modeling And Simulation Of A Floating Oscillating Water Column," in *Proceedings of the ASME 2011 30th International Conference on Ocean, Offshore and Arctic Engineering*, Rotterdam, The Netherlands, 2011.

[18] *WAMIT v6.4*. Chestnut Hill, Massachusetts: WAMIT, Inc.

[19] *3D CAD Design Software SolidWorks*. Dassault Systèmes SolidWorks Corp.

[20] *MultiSurf*. Southwest Harbor, Maine: AeroHydro, Inc.

[21] Y. Imai, K. Toyota, S. Nagata, T. Setoguchi, and M. Takao, "An Experimental Study on Generating Efficiency of a Wave Energy Converter" Backward Bent Duct Buoy," presented at the EWTEC.

[22] M. Suzuki, T. Kuboki, S. Nagata, and T. Setoguchi, "Numerical Investigation of 2D Optimal Profile of Backward-Bent Duct Type Wave Energy Converter," *J. Offshore Mech. Arct. Eng.*, vol. 133, no. 4, pp. 041602–8, Nov. 2011.

[23] D. Hong, S. Hong, and S. Hong, "Numerical study on the reverse drift force of floating BBDB wave energy absorbers," *Ocean engineering*, vol. 31, no. 10, pp. 1257–1294, 2004.

[24] Copeland, Guild and Bull, Diana, "BBDB Structural Model: Simplified Modular Design." Internal Report. Not Yet Published.

[25] Epler, Jeff, "OWC Device Components, Dimensions, Design Standards, Mass & Inertia Estimates," ReVision Consulting, 25-Jan-2012. Internal Report. Not Yet Published.

[26] Previsic, Mirko, "OWC Power Conversion Chain Weight Estimate," 10-Jan-2012. Private communication.

[27] J. N. Newman, *Marine hydrodynamics*. MIT Press, 1977.

[28] A. Brendmo, J. Falnes, and P. Lillebekken, "Linear modelling of oscillating water columns including viscous loss," *Applied ocean research*, vol. 18, no. 2, pp. 65–75, 1996.

[29] M. A. de A. Alves, "Numerical Simulation of the Dynamics of Point Absorber Wave Energy Converters using Frequency and Time Domain Approaches," UNIVERSIDADE TÉCNICA DE LISBOA, INSTITUTO SUPERIOR TÉCNICO, 2011.